

Intrinsic point defects and the n - and p -type dopability of the narrow gap semiconductors GaSb and InSb

J. Buckeridge,^{1,*} T. D. Veal,² C. R. A. Catlow,¹ and D. O. Scanlon^{1,3,4}

¹*University College London, Kathleen Lonsdale Materials Chemistry,
Department of Chemistry, 20 Gordon Street, London WC1H 0AJ, United Kingdom*

²*Stephenson Institute for Renewable Energy and Department of Physics,
School of Physical Sciences, University of Liverpool, Liverpool L69 7ZF, United Kingdom*

³*Diamond Light Source Ltd., Diamond House, Harwell Science and Innovation Campus,
Didcot, Oxfordshire OX11 0DE, United Kingdom*

⁴*Thomas Young Centre, University College London,
Gower Street, London WC1E 6BT, United Kingdom*

The presence of defects in the narrow-gap semiconductors GaSb and InSb affects their dopability and hence applicability for a range of optoelectronic applications. Here, we report hybrid density functional theory based calculations of the properties of intrinsic point defects in the two systems, including spin orbit coupling effects, which influence strongly their band structures. With the hybrid DFT approach we adopt, we obtain excellent agreement between our calculated band dispersions, structural, elastic and vibrational properties and available measurements. We compute point defect formation energies in both systems, finding that antisite disorder tends to dominate, apart from in GaSb under certain conditions, where cation vacancies can form in significant concentrations. Calculated self-consistent Fermi energies and equilibrium carrier and defect concentrations confirm the intrinsic n - and p -type behaviour of both materials under anion-rich and anion-poor conditions. Moreover, by computing the compensating defect concentrations due to the presence of ionised donors and acceptors, we explain the observed dopability of GaSb and InSb.

I. INTRODUCTION

GaSb and InSb belong to the family of III-V, zinc blende structured semiconductors of interest from both a fundamental and technological point of view. The incorporation of Sb in III-V semiconducting nitrides, phosphides and arsenides results in a red shift of the band gap, opening up the possibility of pushing the frequency domain of devices based on such materials far into the infrared (IR).^{1–3} Both GaSb and InSb have applications in long wavelength telecommunications,⁴ high speed microelectronics^{5–7} and optoelectronics.^{8,9} Due to favourable lattice matching, GaSb can be used as a substrate for a wide range of ternary and quaternary III-V compounds.^{10–13} The spin-orbit interaction (SOI) has a strong effect on the valence band structure of both systems,^{14–16} but is more pronounced in InSb,^{17,18} which, combined with a large Landé g -factor (over 50),¹⁹ has meant that InSb has attracted considerable attention in the field of Majorana physics.^{20,21} Moreover, GaSb and InSb have both been demonstrated to incorporate N and Bi effectively, resulting in a reduction in band gap^{22–38} in a similar manner to the more widely studied, GaAs-based dilute nitrides and bismides.^{39,40} Alloys can be produced of GaAs, GaSb and InSb, together with the relevant nitrides and/or bismides to tune the optical and electronic properties for a variety of applications;^{41–45} indeed, very high efficiency tandem solar cells include an active layer composed of such an alloy.⁴⁶

Given the importance of GaSb and InSb, there are surprisingly few studies on their intrinsic defect properties, which are key to their dopability and hence functionality in devices. As-grown GaSb has been shown to be p -

type regardless of growth conditions,^{12,16,47–50} although the acceptor concentrations can be decreased slightly by varying the V/III flux when growing with molecular beam epitaxy (MBE).^{51,52} Gallium vacancies (V_{Ga}) have been shown to occur in GaSb using positron annihilation spectroscopy (PAS),⁵³ but have been ruled out as the dominant acceptor; instead, it has been inferred in further PAS studies that the gallium antisite (Ga_{Sb}) is responsible for the observed p -type activity,^{54,55} based on earlier density functional theory (DFT) calculations using the local density approximation (LDA).⁵⁶ While the LDA was also used to investigate the rôle of H in GaSb,⁵⁷ this approach suffers from the well-known band gap underestimation error, which is particularly problematic in narrow gap semiconductors such as GaSb and InSb. To overcome the band gap error, a subsequent study on defects in GaSb employed hybrid DFT (without including the SOI).⁵⁸ The results, however, indicated that the intrinsic defect physics would result in a semi-insulating material as-grown, in contrast to experiment. C and O impurities were instead proposed to account for the p -type activity.

There are even fewer studies of the defect properties of InSb. The material can be made n - or p -type depending on growth conditions, while temperature (T) dependent studies have been employed to study variations in the n -type carrier concentration, Fermi energy and mobilities in order to elucidate various defect properties.^{50,59–63} A computational study using DFT with the LDA indicated that the antimony antisite (Sb_{In}) would dominate in Sb-rich growth conditions,⁶⁴ by varying growth conditions, it was suggested that the formation of this defect could be suppressed in epitaxially grown thin films.⁶³

77 Furthermore, it has been proposed that the formation
78 of indium vacancies as well as Sb_{In} can account for ob-
79 served changes in the electronic properties of InSb grown
80 in varying conditions.⁶⁵ To our knowledge, no compre-
81 hensive study on the intrinsic defects in InSb using hy-
82 brid DFT has yet been performed.

83 In this Paper, we use hybrid DFT, including the SOI,
84 to investigate the dominant native point defects in both
85 GaSb and InSb. As noted above, the SOI strongly af-
86 fects the dispersion of the upper valence bands in both
87 systems; therefore, depending on the composition of the
88 particular defect states, can have a significant effect on
89 the defect formation energies. We tune the fraction of ex-
90 act exchange in the hybrid functional to reproduce only
91 the band gaps, and justify this approach by computing
92 a range of bulk properties of both systems, demonstrat-
93 ing close agreement with experiment for the structural,
94 electronic, elastic and lattice vibrational properties. Our
95 results show that GaSb will be p -type when grown in
96 Sb-poor conditions, but may be semi-insulating under
97 Sb-rich conditions. InSb, in contrast, will be n -type un-
98 der Sb-poor conditions and p -type under Sb-rich condi-
99 tions. From our computed defect formation energies, we
100 determine self consistent Fermi energies and equilibrium
101 carrier and defect concentrations as a function of T , by
102 imposing the constraint of charge neutrality, calculating
103 concentrations that agree well with experiment. More-
104 over, by introducing fixed concentrations of fully ionised
105 dopants into the self-consistent Fermi energy calculation,
106 we investigate donor and acceptor compensation by na-
107 tive defects in both systems. We find that, while InSb
108 can be easily n - or p -doped, GaSb cannot be effectively
109 n -doped under Sb-poor conditions. We provide the first
110 comprehensive study of intrinsic disorder in GaSb and
111 InSb using relativistic hybrid DFT which helps to eluci-
112 date the defect properties and dopability of both systems
113 under equilibrium conditions.

114 The rest of the paper is structured as follows: In Sec-
115 tion II, we describe our computational methodology.
116 We present our results in Section III and summarize our
117 main findings in Section IV.

118 II. CALCULATIONS

119 To calculate the bulk and defect properties of GaSb
120 and InSb, we have used plane-wave DFT as implemented
121 in the VASP code,⁶⁶⁻⁶⁹ utilizing the Heyd-Scuseria-
122 Ehrnzerof (HSE06) hybrid density functional⁷⁰ for elec-
123 tron exchange and correlation with the projector aug-
124 mented wave method⁷¹ to model the interaction between
125 core and valence electrons (including $3d$ and $4d$ states
126 among the 13 valence electrons in the cases of Ga and
127 In, respectively, and five valence electrons for As). Spin-
128 orbit interactions were included in all calculations.⁷² The
129 proportion α of exact exchange in the hybrid functional
130 was set to $\alpha = 0.335$ ($\alpha = 0.31$) for GaSb (InSb) in order
131 to reproduce the fundamental gap (see below). The total

132 energy of the zinc blende primitive cell was calculated at a
133 series of constant volumes, using a 400 eV plane wave cut
134 off and a $12 \times 12 \times 12$ Γ -centred Monkhorst-Pack⁷³ k -point
135 mesh (a finer $14 \times 14 \times 14$ k -point grid was used when com-
136 puting the density of states (DOS)), which provided con-
137 vergence in the total energy up to 10^{-4} eV, fitting the
138 resultant energy-volume data to the Murnaghan equa-
139 tion of state. The bulk modulus B_0 was derived using
140 this approach. The zone-centre longitudinal phonon fre-
141 quencies (ω_{LO}) were calculated using the frozen phonon
142 approach, as implemented in VASP.⁷⁴ We have also com-
143 puted the elastic constants C_{11} , C_{12} and C_{44} , using the
144 finite displacement approach available in VASP. Electron
145 (m_e^*), light hole (m_{lh}^*) and heavy hole (m_{hh}^*) effective
146 masses were calculated by fitting quadratic functions to
147 the energy dispersion within 1 meV of the appropriate
148 band extremum. For the hole masses, derived from the
149 valence bands where the dispersion is non-spherical, we
150 took an average of the values obtained for the different
151 cartesian directions.

152 Defect calculations were performed using the supercell
153 approach with a 64-atom $2 \times 2 \times 2$ expansion of the con-
154 ventional cubic cell, which has been shown to be suitably
155 converged previously.^{36,57,58,75-77} The formation energy
156 of defect X in charge state q , $E_f(X^q)$, was determined
157 through calculation of the heat of formation of the rele-
158 vant defect reaction:^{78,79}

$$E_f(X^q) = E_{\text{tot}}(X^q) - E_{\text{tot}}(\text{bulk}) - \sum_i n_i \mu_i + q(E_{\text{VBM}} + \Delta + E_F) + E_c, \quad (1)$$

159 where $E_{\text{tot}}(X^q)$ ($E_{\text{tot}}(\text{bulk})$) is the total energy of the
160 defect-containing (pure bulk) supercell, E_{VBM} is the en-
161 ergy at the valence band maximum (VBM), E_F is the
162 Fermi energy (introduced as a parameter), Δ is the en-
163 ergy required to align the electrostatic potential in the
164 defect supercell with that of bulk and E_c is a correction
165 term to account for supercell errors such as image charge
166 interactions and, where applicable, erroneous band fill-
167 ing by delocalised carriers. To calculate Δ and E_c , we
168 follow the procedure outlined by Lany *et al.*,⁸⁰ which
169 has been shown to result in corrections closely matched
170 to those derived from full solutions to Poisson's equa-
171 tion.⁸¹ n_i is the number of species i that is added to
172 ($n_i > 0$) or removed from ($n_i < 0$) the supercell to form
173 X , and μ_i is the chemical potential of species i , taken
174 with reference to the calculated standard state energies
175 E_i so that $\mu_i = E_i + \Delta\mu_i$.⁸² The values of $\Delta\mu_i$ can vary
176 depending on the environmental conditions in thermo-
177 dynamic equilibrium, but are constrained by the rela-
178 tion $\Delta\mu_{\text{M}} + \Delta\mu_{\text{Sb}} = \Delta H[\text{MSb}]$, where $\text{M}=\text{Ga}$ or In and
179 $\Delta H[\text{MSb}]$ is the heat of formation of MSb; we calcu-
180 late $\Delta H[\text{GaSb}] = -0.507$ eV and $\Delta H[\text{InSb}] = -0.470$
181 eV, which are in reasonable agreement with the experi-
182 mental values of -0.433 eV and -0.316 eV, respectively,⁸³
183 particularly taking into account that the experimental
184 values correspond to room T , while the calculations are
185 done at the athermal limit (one would expect the heats

186 of formation to become more negative by ~ 0.05 eV⁸³ at
 187 0 K).⁸⁴ We calculate the $E_f[X]$ at two extremes: Sb rich,
 188 where $\Delta\mu_{\text{Sb}} = 0$ eV, corresponding to an excess of Sb in
 189 the growth environment and absence of pure In, and Sb
 190 poor, the opposite extreme, where $\Delta\mu_{\text{Sb}} = \Delta H[\text{MSb}]$.

191 From the calculated defect formation energies and
 192 DOS, we used the code SC-FERMI^{85–88} to determine the
 193 equilibrium carrier and defect concentrations. SC-FERMI
 194 employs Fermi-Dirac statistics to calculate the concentra-
 195 tions, which are functions of E_F . With the constraint of
 196 overall charge neutrality in the system, a self-consistent
 197 E_F can be derived at any temperature and consequently
 198 so can the electron (n_0), hole (p_0) and defect ($[X]$) con-
 199 centrations. Moreover, the charge neutrality constraint
 200 can be exploited in order to introduce fixed concentra-
 201 tions of ionised impurities, and the equilibrium carrier
 202 and defect concentrations recalculated in the presence of
 203 such impurities. In such a way, one can analyse ionised
 204 donor and acceptor compensation. In our calculations we
 205 neglect the temperature dependence of the free energies
 206 of defect formation due to the high computational cost
 207 in determining the associated vibrational entropy; one
 208 would expect the free energies to change by $\sim 0.1 - 0.2$
 209 eV over the temperature range we employ, but including
 210 such changes would not affect significantly the conclu-
 211 sions we draw from our results.

212 III. RESULTS

213 A. Bulk properties

214 In Table I, we show our calculated lattice parameter
 215 a , B_0 , elastic constants C_{11} , C_{12} and C_{44} , band gap E_g ,
 216 spin-orbit split off energy Δ_{SO} , m_e^* , m_{lh}^* , m_{hh}^* and ω_{LO}
 217 for GaSb and InSb, compared with experiment.^{59,89–101}
 218 As described above, the α used in the hybrid functional
 219 was chosen to reproduce the band gap at low T . From
 220 Table I, however, we see that the hybrid DFT approach
 221 reproduces very well the experimental structural, elastic,
 222 and lattice vibrational properties of both materials,
 223 while the energy dispersion derived properties are also
 224 well reproduced. The only significant discrepancies oc-
 225 cur for InSb, particularly in B_0 and ω_{LO} , indicating a
 226 slightly softer lattice in the calculation compared with
 227 experiment. The calculated m_{hh}^* for InSb is significantly
 228 lower than the experimental value, but this discrepancy
 229 may be due to difficulties in measuring this property ac-
 230 curately. Overall, the agreement between the calculated
 231 values and experiment is satisfactory, and indicates that
 232 our DFT approach is appropriate.

233 In Fig. 1, we show our hybrid-DFT-computed band
 234 structures of GaSb and InSb compared with experimen-
 235 tal values determined using angle-resolved photoemission
 236 spectroscopy (ARPES) and, for the case of GaSb, re-
 237 flectance measurements.^{93,102–104} For GaSb, we have also
 238 calculated band energies using the fully self consistent
 239 GW approach, as implemented in VASP,^{105–107} includ-

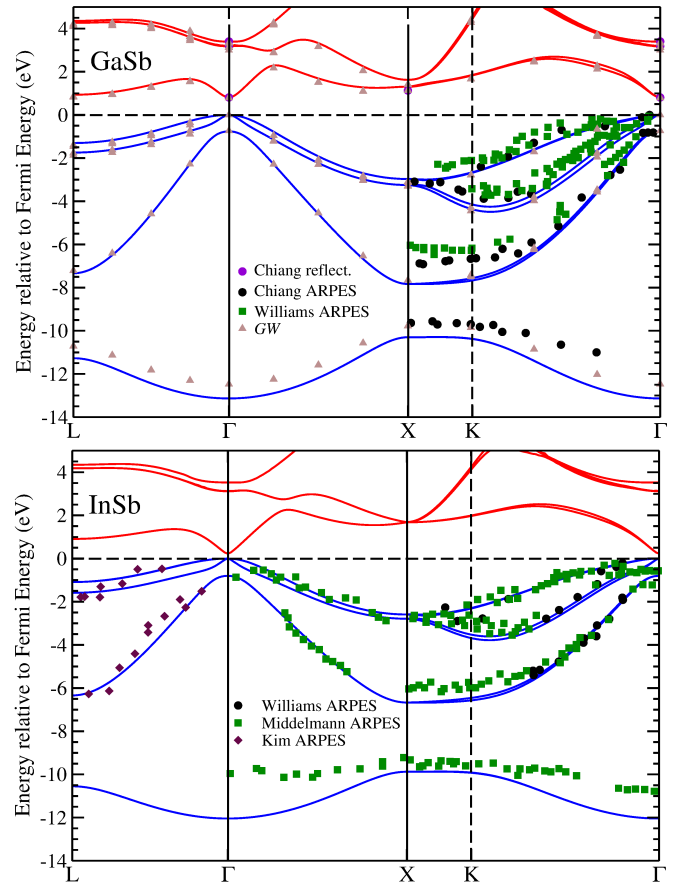


FIG. 1. (Color online) Band structure of GaSb and InSb calculated using hybrid density functional theory (valence bands indicated by blue lines, conduction bands by red lines), compared with experimental results determined for the case of GaSb using reflectance measurements by Chiang and Eastman⁹³ (purple circles) and angle-resolved photoemission spectroscopy (ARPES, black circles and green squares) by Chiang and Eastman⁹³ and Williams *et al.*¹⁰², as well as calculated energy levels using self-consistent GW (brown triangles). The InSb bands are compared with ARPES measurements by Williams *et al.*¹⁰² (black circles), Middelmann *et al.*¹⁰³ (green squares) and Kim *et al.*¹⁰⁴ (maroon diamonds).

240 ing the SOI. As these calculations are computationally
 241 expensive, we have not determined the dispersion along
 242 the high symmetry path in the Brillouin zone with as
 243 small a grid spacing as we have for the hybrid DFT cal-
 244 culations. The band structure is similar in both cases to
 245 GaAs,¹⁰⁸ with the VBM and conduction band minimum
 246 (CBM) both occurring at the Γ point, and a splitting of
 247 the 6-fold degenerate upper valence bands into 4-fold and
 248 2-fold degenerate bands, the latter forming the spin-orbit
 249 split-off bands. For both systems, the hybrid DFT ap-
 250 proach reproduces the band structure well, apart from
 251 the lower-lying Sb s states (at about -11 eV), which are
 252 deeper than either experiment or the GW results. The
 253 bands near the VBM and the conduction band minimum

TABLE I. Calculated lattice parameter a , bulk modulus B_0 , elastic constants C_{11} , C_{12} and C_{44} , band gap E_g , spin-orbit split off energy Δ_{SO} , electron (m_e^*), light hole (m_{lh}^*) and heavy hole (m_{hh}^*) effective masses and zone-centre longitudinal optical phonon frequency ω_{LO} of GaSb and InSb, compared with experimental results.^{59,89–101} The effective masses are given in units of the electronic rest mass.

	a (Å)	B_0 (GPa)	C_{11} (GPa)	C_{12} (GPa)	C_{44} (GPa)	E_g (eV)	Δ_{SO} (eV)	m_e^*	m_{lh}^*	m_{hh}^*	ω_{LO} (cm ⁻¹)	
GaSb	Calc.	6.137	55.1	92.33	39.03	45.99	0.808	0.76	0.041	0.047	0.23	230.4
	Expt.	6.09593 ⁸⁹	56.35 ⁹⁰	90.82 ⁹¹	41.31 ⁹¹	44.47 ⁹¹	0.813 ⁹²	0.82 ⁹³	0.0412 ⁹⁴	0.05 ⁹⁵	0.28 ⁹⁵	232.6 ⁹⁶
InSb	Calc.	6.548	40	68.2	33.8	31.6	0.23	0.80	0.018	0.019	0.25	180.3
	Expt.	6.4794 ⁹⁷	48.1 ⁹⁸	69.18 ⁹⁸	37.88 ⁹⁸	31.32 ⁹⁸	0.24 ⁹⁹	0.80 ⁹⁹	0.015 ⁵⁹	0.015 ¹⁰⁰	0.43 ¹⁰⁰	196.8 ¹⁰¹

(CBM), however, are very well reproduced. These bands are the most significant for defect state formation.

B. Defects in GaSb

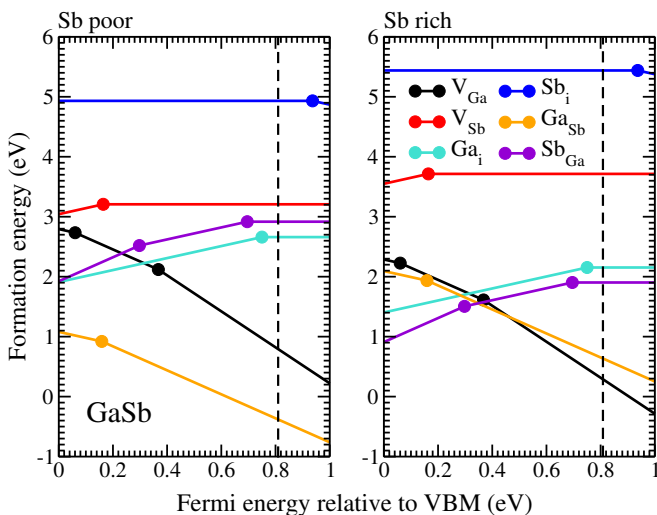


FIG. 2. (Color online) Calculated formation energies of each intrinsic defect (vacancies, interstitials and antisites; see text for description) in GaSb as a function of Fermi energy relative to the valence band maximum (VBM), shown for Sb-poor and Sb-rich conditions. The slope of each line indicates the defect charge state; the transition levels lie where the slopes change. The dashed line indicates the position of the conduction band minimum.

Our calculated formation energies of intrinsic defects in GaSb are shown in Fig. 2 as a function of E_F , referenced to the VBM, for Sb-poor and Sb-rich conditions. GaSb dominates in Sb-poor conditions; it has a formation energy under 1 eV and is negatively charged for all values of E_F within the band gap, with an adiabatic transition from the $-$ to $2-$ state, ($-/2-$), occurring at $E_F = 0.16$ eV above the VBM. Such a low energy, negatively charged defect indicates an intrinsically p -type material, as is observed experimentally.^{12,16,47–49} All other defects have formation energies of at least 1 eV higher than GaSb for E_F within the band gap. Previous calcu-

lations by Hakala *et al.*, using DFT-LDA,⁵⁶ and Virkkala *et al.*,⁵⁸ using hybrid DFT, both found that GaSb had the lowest formation energy for E_F in the upper half of the band gap, but predicted compensation by Ga interstitials (Ga_i^+), resulting in an insulating material. The LDA calculations did not include the SOI nor any correction for the band gap underestimation, while the hybrid DFT calculations did not include the SOI and used higher convergence criteria than those we employ;⁵⁸ their results contradict the experimentally observed p -type activity of undoped GaSb.

In Sb-rich conditions, we find that $E_f(\text{GaSb})$ increases significantly, while $E_f(V_{\text{Ga}})$ and $E_f(\text{Sb}_{\text{Ga}})$ both decrease, so that the lowest energy defects are Sb_{Ga} for $E_F < 0.36$ eV and V_{Ga} for $E_F > 0.42$ eV, with GaSb having the lowest energy for E_F between these ranges. As Sb_{Ga} are positively charged and GaSb and V_{Ga} negatively charged for E_F within the band gap, these defects self compensate and one would expect E_F to remain trapped roughly mid-gap, resulting in an intrinsically insulating material (we note that the formation energy of Ga_i is also low in this range of E_F and we expect that this defect will play a minor rôle in the self-compensation mechanism). These formation energies suggest significant concentrations of V_{Ga} will be present, in agreement with PAS studies,^{53–55,109} but the insulating nature contradicts the p -type activity of GaSb observed in many differently produced samples. It may be the case that, in non-equilibrium growth techniques, formation of the compensating Sb_{Ga} may be suppressed, which would result in a p -type material where the hole concentration arises from the ionisation of V_{Ga} and GaSb.^{51,52} Our results for Sb-rich conditions agree qualitatively with those of Virkkala *et al.*,⁵⁸ although they did not predict that the V_{Ga} would become the lowest energy defect for any value of E_F within the band gap. Comparisons with the LDA calculations of Hakala *et al.*⁵⁶ are more difficult, as they only reported formation energies for Sb_{Ga} in the neutral state. We note, however, that they also found V_{Ga} to be the lowest energy defect close to the conduction band minimum (CBM).

From our computed defect formation energies and total DOS, we have calculated the self-consistent E_F and equilibrium carrier and defect concentrations by applying the constraint of overall charge neutrality to our system. The results are shown in Fig. 3(a) over the T range below the melting point (985 K⁸³). It is worth noting here that,

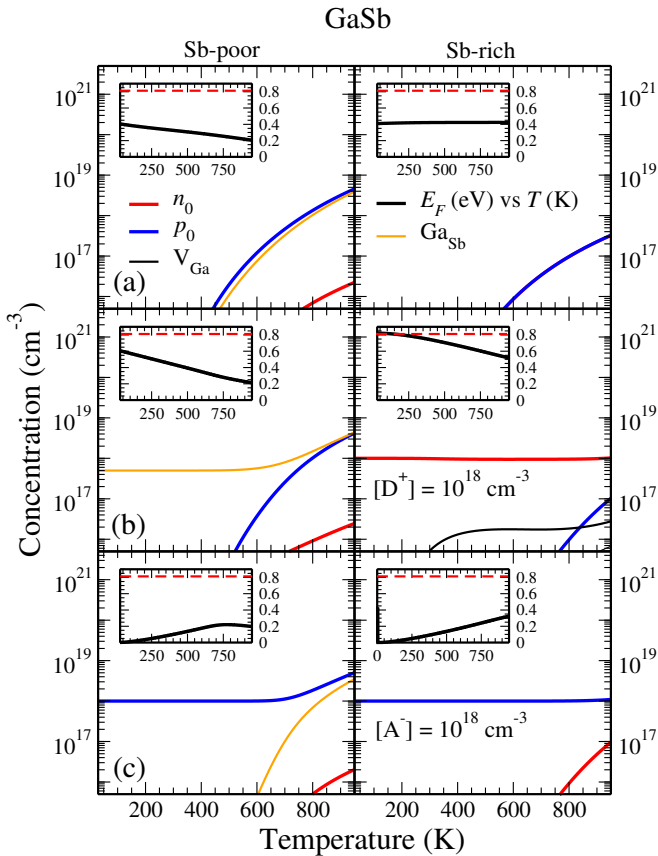


FIG. 3. (Color online) Concentrations of electron (n_0) and hole (p_0) carriers and defects (vacancies, interstitials and antisites; see text for description) in GaSb as a function of temperature T calculated for (a) equilibrium conditions, (b) in the presence of a fixed concentration of donors $[D^+] = 10^{18} \text{ cm}^{-3}$ and (c) a fixed concentration of acceptors $[A^+] = 10^{18} \text{ cm}^{-3}$. The results are shown for Sb-poor and Sb-rich conditions in the left- and right-side panels, respectively. The insets show the self-consistent Fermi energy E_F as a function of T , with the conduction band minimum indicated by the red dashed line.

when varying T in this analysis and for the case of InSb below we do not take into account the variation in band gap, which can be substantial for these narrow gap semiconductors. Indeed, at room temperature the band gap reduces by 86 meV for GaSb¹ and 67 meV for InSb,⁹⁹ compared with their extrapolated 0 K values. Such reductions are a result of thermal expansion and increased electron-phonon coupling, the modelling of which is beyond the scope of this study on defects in both systems. Including the experimental variation in E_g with T in our calculations is not straightforward, as the defect transition levels vary with T in a non-trivial manner. If we do include just the experimental E_g variation, we calculate slightly different electron and hole concentrations which do not alter our conclusions significantly. As modelling temperature effects on the defect formation and

transition levels is beyond the scope of the current work, we present our analysis below with the band gap fixed for all temperatures studied. We expect that, at higher T , where the band gap is reduced and consequently the electron and hole concentrations increased, compensating defect formation energies will also be lowered as vibrational entropy contributions to the free energy become more significant, so that the changes in concentrations will approximately cancel each other.

From our analysis we find that, in Sb-poor conditions, GaSb is p -type with hole concentrations p_0 of $\sim 10^{16} - 10^{18} \text{ cm}^{-3}$ for $400 < T < 800 \text{ K}$. The source of the p_0 is the formation and ionisation of Ga_{Sb} ; p_0 is equal to $2[\text{Ga}_{\text{Sb}}]$, which is consistent with the dominant charge state of Ga_{Sb} being $2-$, but at $T \approx 800 \text{ K}$ the concentrations become close to being equal, as E_F moves closer to the VBM where the $-$ state dominates. These calculated hole concentrations are lower by about an order of magnitude than those seen in experiment,^{48,49} the discrepancy may be due to unwanted impurities such as C that can be introduced during experimental growth, which are not accounted for here. p_0 and $[\text{Ga}_{\text{Sb}}]$ are also about an order magnitude lower than those computed by Hakala *et al.*,⁵⁶ which can be attributed to their lower value of $E_f(\text{Ga}_{\text{Sb}}^{2-})$. The difference in formation energies is probably due to a combination of the difference in functional and in the more crude image charge corrections used in their much earlier work. In Sb-rich conditions, we find that E_F remains trapped at about 0.4 eV above the VBM over the range of T investigated, due to the self-compensating defect physics, whereby the combined concentration of Sb_{Ga}^+ , $\text{Sb}_{\text{Ga}}^{2+}$ and Ga_i^+ equals that of V_{Ga}^- , V_{Ga}^{2-} and $\text{Ga}_{\text{Sb}}^{2-}$, with the individual proportions depending on T . Consequently, the electron concentration n_0 is equal to p_0 and the material is intrinsically insulating. This insulating nature is rarely seen experimentally; again, unwanted p -type impurities not included in this study, as well as non-equilibrium defect formation, expected to be important in samples grown epitaxially where kinetics dominate,^{16,49} may account for the discrepancy.

When imposing the charge neutrality constraint to determine the self-consistent E_F , it is possible to introduce fixed concentrations of other charged defects and calculate the equilibrium carrier and intrinsic defect concentrations in their presence. In this way, one can analyse compensation of fully ionised impurities in an approximate manner. By assuming a fixed concentration of some ionised donor, $[D^+] = 10^{18} \text{ cm}^{-3}$, we have calculated donor compensation in GaSb, with our results shown in Fig. 3(b). We find that, in Sb-poor conditions, rather than introducing n -type carriers, the donors are compensated by $\text{Ga}_{\text{Sb}}^{2-}$, so that $[D^+] = 2[\text{Ga}_{\text{Sb}}]$ for $T < 600 \text{ K}$. We see, therefore, that in Sb-poor conditions donor doping will not be effective, assuming that defect formation occurs in equilibrium. In fact, p_0 will become greater than 10^{16} cm^{-3} at about $T = 600 \text{ K}$, and continues to rise with temperature as $[\text{Ga}_{\text{Sb}}]$ increases above the value

389 necessary to compensate $[D^+]$ due to thermal activation,
 390 while E_F is pushed closer to the VBM. In Sb-rich con-
 391 ditions, however, we have $[D^+] = n_0$ for most of the
 392 temperature range studied, so that GaSb will be doped
 393 effectively. At lower temperature, E_F remains close to
 394 the CBM, but decreases into the band gap with increas-
 395 ing temperature. There is a very small dip in n_0 around
 396 $T = 400$ K, which occurs as thermally induced concen-
 397 trations of V_{Ga} compensate slightly the donors. We note
 398 that, in MBE-grown samples intentionally doped n -type,
 399 increasing the V/III ratio (i.e. going towards increas-
 400 ingly Sb-rich conditions) caused a slight increase in com-
 401 pensating acceptor concentrations,^{51,52} contrary to our
 402 findings here. The effect is small and may be due to
 403 non-equilibrium defect formation and/or the presence of
 404 unwanted impurities.

405 In the same way, we can analyse acceptor compensa-
 406 tion in GaSb. In Fig. 3(c), we show the equilibrium car-
 407 rier and intrinsic defect concentrations in the presence of
 408 a fixed concentration of an ionised acceptor, $[A^-] = 10^{18}$
 409 cm^{-3} . The situation here is quite different to donor com-
 410 pensation discussed above; in both Sb-poor and Sb-rich
 411 conditions the acceptors are uncompensated and we have
 412 a p -type material with $p_0 = [A^-]$. E_F remains close to
 413 the VBM, but moves towards mid-gap as T increases,
 414 as one would expect due to T -induced intrinsic carrier
 415 generation. In Sb-poor conditions, for $T > 600$ K, sub-
 416 stantial concentrations of Ga_{Sb} form, which further con-
 417 tribute to the p -type activity. We therefore find that
 418 GaSb can be effectively p -doped, whether in Sb-rich or
 419 Sb-poor conditions, a result that is consistent with ex-
 420 periment.

421 C. Defects in InSb

422 We show our calculated intrinsic defect formation ener-
 423 gies as a function of E_F referenced to the VBM in Fig. 4.
 424 We find that, in contrast to the case of GaSb, we have
 425 a positively charged defect, Sb_{In} , dominating in Sb-rich
 426 conditions and a negatively charged defect, In_{Sb} , domi-
 427 nating in Sb-poor conditions. Consequently, one would
 428 expect an n -type material if grown in Sb-rich conditions,
 429 and a (weakly, due to the relatively high formation en-
 430 ergy) p -type material if grown in Sb-poor conditions. Ex-
 431 perimentally, both n - and p -type unintentionally doped
 432 samples are routinely prepared, and InSb can be doped
 433 relatively easily with electrons or holes as majority car-
 434 riers.^{50,59-63} Hoglund *et al.*⁶⁴ calculated the defect forma-
 435 tion energies using DFT-LDA, finding results consistent
 436 with ours for Sb-rich conditions, but for the Sb-poor con-
 437 ditions they found that In_i would dominate, resulting in
 438 an n -type material, in contrast to our results. In their
 439 calculations, they found InSb to be gapless, contradict-
 440 ing experiment, and did not discuss corrections for this
 441 error nor for image charge interactions in their supercell
 442 model. The Sb_{In} defect has been proposed to be a source
 443 of intrinsic n -type carriers in epitaxially grown InSb, but

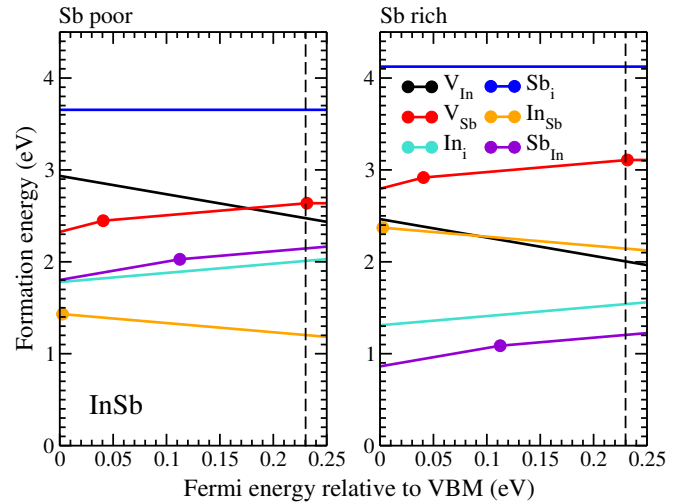


FIG. 4. (Color online) Calculated formation energies of each intrinsic defect (vacancies, interstitials and antisites; see text for description) in InSb as a function of Fermi energy relative to the valence band maximum (VBM), shown for Sb-poor and Sb-rich conditions. The slope of each line indicates the defect charge state; the transition levels lie where the slopes change. The dashed line indicates the position of the conduction band minimum.

444 can be removed effectively by decreasing the V/III ra-
 445 tio, i.e. moving away from Sb-rich conditions.⁶³ Such an
 446 observation is consistent with our calculated formation
 447 energies. Vacancies have also been proposed to be im-
 448 portant in InSb,^{65,110-112} but our results show that their
 449 concentrations should be small as their formation en-
 450 ergies are relatively high. We note that, although we have
 451 pointed out some differences between the defect physics
 452 of InSb and GaSb, some of these differences can be traced
 453 to the much lower band gap of InSb, compared with GaSb
 454 (0.23 eV *vs* 0.808 eV). Restricting the range of E_F to re-
 455 main less than 0.23 eV in GaSb would result in a similar
 456 transition level diagram to that of InSb. This result indi-
 457 cates a small valence band offset between the materials,
 458 consistent with earlier studies.^{14,97,113}

459 As with the case of GaSb, we have calculated equilib-
 460 rium carrier and defect concentrations in InSb (exclud-
 461 ing the variation in E_g with T , see the discussion above);
 462 our results are shown in Fig. 5(a) over the T range be-
 463 low the melting point (797 K⁸³). Despite the dominance
 464 of positively and negatively charged defects in Sb-rich
 465 and Sb-poor conditions respectively, we find that, under
 466 either condition InSb will be insulating as-grown. This
 467 result is a consequence of the low band gap and relatively
 468 high defect formation energies; thermally induced intrin-
 469 sic carrier formation will dominate as defect concentra-
 470 tions remain several orders of magnitude below the car-
 471 rier concentrations over the relevant T range (in Sb-poor
 472 conditions, $[\text{In}_{\text{Sb}}]$, not shown in the figure, rises above
 473 10^{14} cm^{-3} only for $T > 700$ K). E_F remains closer to the

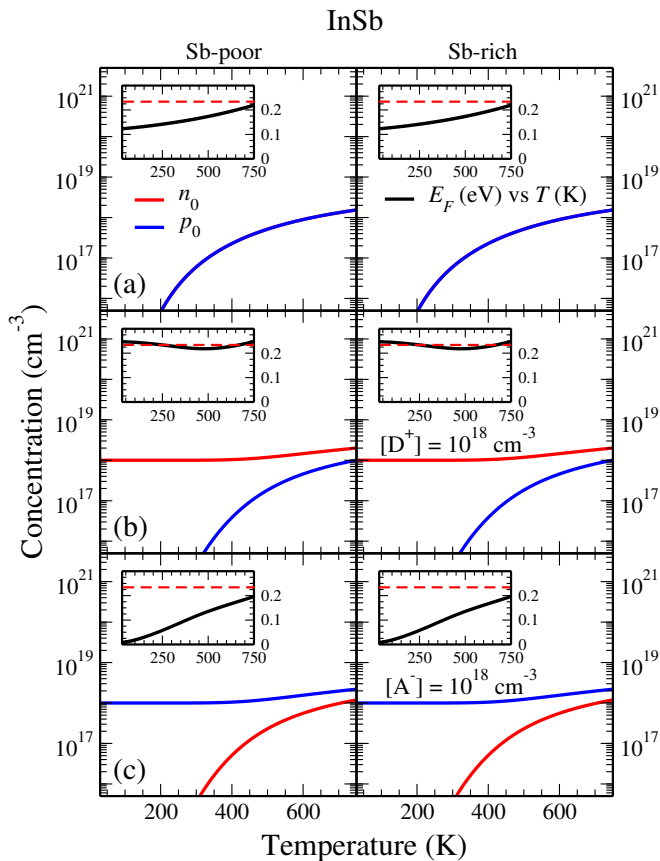


FIG. 5. (Color online) Concentrations of electron (n_0) and hole (p_0) carriers and, defects (vacancies, interstitials and antisites; see text for description) in InSb as a function of temperature T calculated for (a) equilibrium conditions, (b) in the presence of a fixed concentration of donors $[D^+] = 10^{18} \text{ cm}^{-3}$ and (c) a fixed concentration of acceptors $[A^+] = 10^{18} \text{ cm}^{-3}$. The results are shown for Sb-poor and Sb-rich conditions in the left- and right-side panels, respectively. The insets show the self-consistent Fermi energy E_F as a function of T , with the conduction band minimum indicated by the red dashed line.

474 CBM, as the DOS at the bottom of the conduction band
 475 is much lower than that at the top of the valence band.
 476 To produce n - and p -type samples therefore, one needs to
 477 dope the material and nominally undoped samples that
 478 have substantial carrier concentrations probably have un-
 479 wanted impurities present, according to our results.

480 In Fig. 5(b) we show the equilibrium carrier and defect
 481 concentrations in the presence of a fixed concentration
 482 of ionised donors, $[D^+] = 10^{18} \text{ cm}^{-3}$. In both Sb-poor
 483 and Sb-rich conditions, we find that InSb can be donor
 484 doped effectively, resulting in $n_0 = [D^+]$ for much of the
 485 T range. As the DOS is relatively low at the CBM, to
 486 induce the relevant electron concentration E_F is pushed
 487 very up to the CBM (see the inset in Fig. 5(b)). No
 488 significant defect compensation is observed; indeed, we
 489 find that, for $T > 400 \text{ K}$, thermal ionisation increases n_0

490 above $[D^+]$.

491 We have also analysed acceptor compensation in InSb
 492 by assuming a fixed ionised acceptor concentration,
 493 $[A^-] = 10^{18} \text{ cm}^{-3}$, and computing the resultant carrier
 494 and defect concentrations; our results are shown in
 495 Fig. 5(c). In both Sb-poor and Sb-rich conditions there
 496 is no effective compensation of the acceptors by defects,
 497 indicating that InSb will be easily acceptor doped in either
 498 extreme condition. E_F varies across the gap as T
 499 increases, which induces minority carrier concentrations
 500 while also increasing the majority carrier concentration.
 501 We therefore see that InSb can be both n - and p -doped
 502 without significant compensation by intrinsic point defect
 503 formation, a result that is consistent with experi-
 504 ment.^{50,63,64}

505 IV. SUMMARY

506 We have investigated the intrinsic defect physics in
 507 GaSb and InSb by computing native defect formation en-
 508 ergies using hybrid DFT. We justify our approach by first
 509 calculating a range of bulk properties of both systems,
 510 obtaining results in good agreement with experiment. We
 511 find that, in GaSb Ga_{Sb} will dominate in Sb-poor con-
 512 ditions, resulting in a p -type material, while in Sb-rich
 513 conditions self-compensation will occur and the material
 514 will be intrinsic. We confirm these inferences from the
 515 formation energy calculations by computing equilibrium
 516 carrier and defect concentrations as a function of tem-
 517 perature, then study donor and acceptor compensation
 518 by assuming fixed concentrations of ionised dopants. We
 519 find that GaSb can be easily p -doped, but in equilib-
 520 rium conditions, should only be effectively n -doped un-
 521 der Sb-rich conditions. For InSb, we find that positively
 522 charged (Sb_{In}) and negatively charged antisite defects
 523 (In_{Sb}) dominate in Sb-rich and Sb-poor conditions, re-
 524 spectively. By calculating equilibrium carrier and defect
 525 concentrations, however, we show that the material will
 526 be intrinsic as-grown, due to the relatively high formation
 527 energies, low band gap and consequent thermally induced
 528 carrier generation. As the concentrations of compensat-
 529 ing defects remain low over the relevant T range, InSb
 530 can be effectively n - and p -doped. Our study provides
 531 crucial information on the defect physics of GaSb and
 532 InSb, important semiconductors for a range of techno-
 533 logical applications.

534 ACKNOWLEDGMENT

535 The authors acknowledge funding from EPSRC grants
 536 ED/D504872, EP/K016288/1 and EP/I01330X/1 and
 537 the European Research Council (grant 758345). The
 538 authors also acknowledge the use of the UCL Le-
 539 gion and Grace High Performance Computing Facil-
 540 ities (Legion@UCL and Grace@UCL) and associated
 541 support services, the IRIDIS cluster provided by the

542 EPSRC funded Centre for Innovation (EP/K000144/1
 543 and EP/K000136/1), the Thomas supercomputer via
 544 the U.K. Materials and Modelling Hub (EPSRC
 545 grant EP/P020194/1) and the ARCHER supercomputer
 546 through membership of the UK's HPC Materials Chem-
 547 istry Consortium, which is funded by EPSRC grants
 548 EP/L000202 and EP/R029431, in the completion of this
 549 work. D. O. S. and T. D. V. acknowledge membership of
 550 the Materials Design Network.

-
- 551 * j.buckeridge@ucl.ac.uk
 552 ¹ P. S. Dutta, H. L. Bhat, and V. Kumar, *J. Appl. Phys.*
 553 **81**, 5821 (1997).
 554 ² A. Rogalski, J. Antoszewski, and L. Faraone, *J. Appl.*
 555 *Phys.* **105**, (2009).
 556 ³ P. Gogoi, D. Kamenskyi, D. D. Arslanov, R. T. Jongma,
 557 W. J. van der Zande, B. Redlich, A. F. G. van der Meer,
 558 H. Engelkamp, P. C. M. Christianen, and J. C. Maan,
 559 *Phys. Rev. Lett.* **119**, 146603 (2017).
 560 ⁴ S. Tomasulo, C. A. Affouda, N. A. Mahadik, M. E. Twigg,
 561 M. K. Yakes, and E. H. Aifer, *J. Vac. Sci. Technol. B* **36**,
 562 02D108 (2018).
 563 ⁵ T. Ashley, A. B. Dean, C. T. Elliott, G. J. Pryce, A. D.
 564 Johnson, and H. Willis, *Appl. Phys. Lett.* **66**, 481 (1995).
 565 ⁶ C. A. Lehner, T. Tschirky, T. Ihn, W. Dietsche, J. Keller,
 566 S. Fält, and W. Wegscheider, *Phys. Rev. Materials* **2**,
 567 054601 (2018).
 568 ⁷ S. Petrosyan and A. Khachatryan, *Semicond. Sci. Technol.*
 569 **34**, 045018 (2019).
 570 ⁸ J. Paaajaste, S. Suomalainen, R. Koskinen, A. Hrknen,
 571 M. Guina, and M. Pessa, *J. Cryst. Growth* **311**, 1917
 572 (2009), International Conference on Molecular Beam Epi-
 573 taxy (MBE-XV).
 574 ⁹ M. Guina, A. Rantamki, and A. Hrknen, *J. Phys. D:*
 575 *Appl. Phys.* **50**, 383001 (2017).
 576 ¹⁰ P. H. Jefferson, L. Buckle, B. R. Bennett, T. D. Veal,
 577 D. Walker, N. R. Wilson, L. F. J. Piper, P. A. Thomas,
 578 T. Ashley, and C. F. McConville, *J. Cryst. Growth* **304**,
 579 338 (2007).
 580 ¹¹ M. J. Ashwin, D. Walker, P. A. Thomas, T. S. Jones, and
 581 T. D. Veal, *J. Appl. Phys.* **113**, 033502 (2013).
 582 ¹² H. Kala, G. A. Umana-Membreno, G. Jolley, N. D. Akha-
 583 van, M. A. Patrashin, K. Akahane, J. Antoszewski, and
 584 L. Faraone, *Appl. Phys. Lett.* **106**, 032103 (2015).
 585 ¹³ U. Serincan and B. Arpapay, *Semicond. Sci. Technol.* **34**,
 586 035013 (2019).
 587 ¹⁴ L. Ley, R. A. Pollak, F. R. McFeely, S. P. Kowalczyk, and
 588 D. A. Shirley, *Phys. Rev. B* **9**, 600 (1974).
 589 ¹⁵ B. Shojaei, A. P. McFadden, M. Pendharkar, J. S. Lee,
 590 M. E. Flatté, and C. J. Palmstrøm, *Phys. Rev. Materials*
 591 **2**, 064603 (2018).
 592 ¹⁶ M. Karalic, C. Mittag, M. Hug, T. Tschirky, W. Wegschei-
 593 der, K. Ensslin, T. Ihn, K. Shibata, and R. Winkler, *Phys.*
 594 *Rev. B* **99**, 115435 (2019).
 595 ¹⁷ G. A. Khodaparast, R. E. Doezema, S. J. Chung, K. J.
 596 Goldammer, and M. B. Santos, *Phys. Rev. B* **70**, 155322
 597 (2004).
 598 ¹⁸ T. Campos, P. E. Faria Junior, M. Gmitra, G. M. Sipahi,
 599 and J. Fabian, *Phys. Rev. B* **97**, 245402 (2018).
 600 ¹⁹ K. L. Litvinenko, L. Nikzad, C. R. Pidgeon, J. Allam,
 601 L. F. Cohen, T. Ashley, M. Emeny, W. Zawadzki, and
 602 B. N. Murdin, *Phys. Rev. B* **77**, 033204 (2008).
 603 ²⁰ V. Mourik, K. Zuo, S. M. Frolov, S. R. Plissard, E. P.
 604 A. M. Bakkers, and L. P. Kouwenhoven, *Science* **336**,
 605 1003 (2012).
 606 ²¹ M. T. Deng, C. L. Yu, G. Y. Huang, M. Larsson, P. Caroff,
 607 and H. Q. Xu, *Nano Lett.* **12**, 6414 (2012).
 608 ²² T. Ashley, T. Burke, G. Pryce, A. Adams, A. Andreev,
 609 B. Murdin, E. O'Reilly, and C. Pidgeon, *Solid-State Elec-*
 610 *tronics* **47**, 387 (2003).
 611 ²³ T. D. Veal, L. F. J. Piper, S. Jollands, B. R. Bennett,
 612 P. H. Jefferson, P. A. Thomas, C. F. McConville, B. N.
 613 Murdin, L. Buckle, G. W. Smith, and T. Ashley, *Appl.*
 614 *Phys. Lett.* **87**, 132101 (2005).
 615 ²⁴ P. H. Jefferson, T. D. Veal, L. F. J. Piper, B. R. Bennett,
 616 C. F. McConville, B. N. Murdin, L. Buckle, G. W. Smith,
 617 and T. Ashley, *Appl. Phys. Lett.* **89**, 111921 (2006).
 618 ²⁵ L. Buckle, B. R. Bennett, S. Jollands, T. D. Veal, N. R.
 619 Wilson, B. N. Murdin, C. F. McConville, and T. Ashley,
 620 *J. Cryst. Growth* **278**, 188 (2005).
 621 ²⁶ T. Ashley, L. Buckle, G. W. Smith, B. N. Murdin, P. H.
 622 Jefferson, L. F. J. Piper, T. D. Veal, and C. F. McConville,
 623 Dilute antimonide nitrides for very long wavelength in-
 624 frared applications, in *Proc. SPIE 6206, Infrared Tech-*
 625 *nology and Applications XXXII*, pages 62060L–62060L–8,
 626 2006.
 627 ²⁷ A. Belabbes, M. Ferhat, and A. Zaoui, *Appl. Phys. Lett.*
 628 **88**, 152109 (2006).
 629 ²⁸ S. Iyer, L. Wu, J. Li, S. Potoczny, K. Matney, and P. R. C.
 630 Kent, *J. Appl. Phys.* **101**, 113508 (2007).
 631 ²⁹ A. Lindsay, E. P. O'Reilly, A. D. Andreev, and T. Ashley,
 632 *Phys. Rev. B* **77**, 165205 (2008).
 633 ³⁰ D. Wang, S. P. Svensson, L. Shterengas, G. Belenky, C. S.
 634 Kim, I. Vurgaftman, and J. R. Meyer, *J. Appl. Phys.* **105**,
 635 014904 (2009).
 636 ³¹ M. J. Ashwin, T. D. Veal, J. J. Bomphrey, I. R. Dunn,
 637 D. Walker, P. A. Thomas, and T. S. Jones, *AIP Adv.* **1**,
 638 032159 (2011).
 639 ³² V. Virkkala, V. Havu, F. Tuomisto, and M. J. Puska,
 640 *Phys. Rev. B* **85**, 085134 (2012).
 641 ³³ J. J. Mudd, N. J. Kybert, W. M. Linhart, L. Buckle,
 642 T. Ashley, P. D. C. King, T. S. Jones, M. J. Ashwin, and
 643 T. D. Veal, *Appl. Phys. Lett.* **103**, 042110 (2013).
 644 ³⁴ M. J. Ashwin, R. J. H. Morris, D. Walker, P. A. Thomas,
 645 M. G. Dowsett, T. S. Jones, and T. D. Veal, *J. Phys. D*
 646 *Appl. Phys.* **46**, 264003 (2013).
 647 ³⁵ M. K. Rajpalke, W. M. Linhart, K. M. Yu, M. Birkett,
 648 J. Alaria, J. J. Bomphrey, S. Sallis, L. F. J. Piper, T. S.
 649 Jones, M. J. Ashwin, and T. D. Veal, *Appl. Phys. Lett.*
 650 **105**, 212101 (2014).
 651 ³⁶ J. Buckeridge, D. O. Scanlon, T. D. Veal, M. J. Ashwin,
 652 A. Walsh, and C. R. A. Catlow, *Phys. Rev. B* **89**, 014107
 653 (2014).
 654 ³⁷ M. P. Polak, P. Scharoch, and R. Kudrawiec, *Semicond.*
 655 *Sci. Technol.* **30**, 094001 (2015).
 656 ³⁸ W. M. Linhart, M. K. Rajpalke, J. Buckeridge, P. A. E.
 657 Murgatroyd, J. J. Bomphrey, J. Alaria, C. R. A. Catlow,
 658 D. O. Scanlon, M. J. Ashwin, and T. D. Veal, *Appl. Phys.*

- 659 Lett. **109**, 132104 (2016).
660 39 E. P. O'Reilly, A. Lindsay, P. J. Klar, A. Polimeni, and
661 M. Capizzi, *Semicond. Sci. Technol.* **24**, 033001 (2009).
662 40 T. F. Kuech, S. E. Babcock, and L. Mawst, *Appl. Phys.*
663 *Rev.* **3**, 040801 (2016).
664 41 A. S. Chang, E. S. Zech, T. W. Kim, Y. H. Lin, L. J.
665 Mawst, and R. S. Goldman, *Appl. Phys. Lett.* **105**,
666 142105 (2014).
667 42 M. Gladysiewicz, R. Kudrawiec, and M. S. Wartak, *J.*
668 *Appl. Phys.* **119**, 075701 (2016).
669 43 Z. Song, S. Bose, W. Fan, D. H. Zhang, Y. Y. Zhang, and
670 S. S. Li, *New J. Phys.* **19**, 073031 (2017).
671 44 P. T. Webster, A. J. Shalindar, S. T. Schaefer, and S. R.
672 Johnson, *Appl. Phys. Lett.* **111**, 082104 (2017).
673 45 K. Kharel and A. Freundlich, *Semicond. Sci. Technol.* **34**,
674 055017 (2019).
675 46 R. Jones-Albertus et al., *MRS Proc.* **1538** (2013).
676 47 H. N. Leifer and W. C. Dunlap, *Phys. Rev.* **95**, 51 (1954).
677 48 Y. V. D. Meulen, *J. Phys. Chem. Solids* **28**, 25 (1967).
678 49 S. K. Haywood, A. B. Henriques, N. J. Mason, R. J.
679 Nicholas, and P. J. Walker, *Semicond. Sci. Technol.* **3**,
680 315 (1988).
681 50 R. Pino, Y. Ko, and P. S. Dutta, *Native Defect Compens-*
682 *ation In III-Antimonide Bulk Substrates*, pages 34–39,
683 World Scientific Publishing Company, 2004.
684 51 M. E. Lee, I. Poole, W. S. Truscott, I. R. Cleverley, K. E.
685 Singer, and D. M. Rohlfling, *J. Appl. Phys.* **68**, 131 (1990).
686 52 G. W. Turner, S. J. Eglash, and A. J. Strauss, *J. Vac.*
687 *Sci. Technol. B* **11**, 864 (1993).
688 53 C. C. Ling, M. K. Lui, S. K. Ma, X. D. Chen, S. Fung,
689 and C. D. Beling, *Appl. Phys. Lett.* **85**, 384 (2004).
690 54 J. Kujala, N. Segercrantz, F. Tuomisto, and J. Slotte, *J.*
691 *Appl. Phys.* **116**, 143508 (2014).
692 55 N. Segercrantz, I. Makkonen, J. Slotte, J. Kujala, T. D.
693 Veal, M. J. Ashwin, and F. Tuomisto, *J. Appl. Phys.* **118**,
694 085708 (2015).
695 56 M. Hakala, M. J. Puska, and R. M. Nieminen, *J. Appl.*
696 *Phys.* **91**, 4988 (2002).
697 57 A. Peles, A. Janotti, and C. G. Van de Walle, *Phys. Rev.*
698 *B* **78**, 035204 (2008).
699 58 V. Virkkala, V. Havu, F. Tuomisto, and M. J. Puska,
700 *Phys. Rev. B* **86**, 144101 (2012).
701 59 H. J. Hrostowski, F. J. Morin, T. H. Geballe, and G. H.
702 Wheatley, *Phys. Rev.* **100**, 1672 (1955).
703 60 S. Zukotyński, S. Graf, and N. Saleh, *Phys. Status Solidi*
704 *B* **42**, K43 (1970).
705 61 K. K. Chen and J. K. Furdyna, *J. Appl. Phys.* **43**, 1825
706 (1972).
707 62 M. Oszwalldowski and M. Zimpel, *J. Phys. Chem. Solids*
708 **49**, 1179 (1988).
709 63 Y. Jin, D. Zhang, X. Chen, and X. Tang, *J. Cryst. Growth*
710 **318**, 356 (2011), The 16th International Conference on
711 Crystal Growth (ICCG16)/The 14th International Confer-
712 ence on Vapor Growth and Epitaxy (ICVGE14).
713 64 A. Höglund, C. W. M. Castleton, M. Göthelid, B. Johans-
714 son, and S. Mirbt, *Phys. Rev. B* **74**, 075332 (2006).
715 65 X.-M. Zhao, Y. Zhang, L.-J. Cui, M. Guan, B.-Q. Wang,
716 Z.-P. Zhu, and Y.-P. Zeng, *Chin. Phys. Lett.* **34**, 076105
717 (2017).
718 66 G. Kresse and J. Hafner, *Phys. Rev. B* **47**, 558 (1993).
719 67 G. Kresse and J. Hafner, *Phys. Rev. B* **49**, 14251 (1994).
720 68 G. Kresse and J. Furthmüller, *Comput. Mater. Sci.* **6**, 15
721 (1996).
722 69 G. Kresse and J. Furthmüller, *Phys. Rev. B* **54**, 11169
723 (1996).
724 70 J. Heyd, G. E. Scuseria, and M. Ernzerhof, *J. Chem.*
725 *Phys.* **124**, 219906 (2006).
726 71 P. E. Blöchl, *Phys. Rev. B* **50**, 17953 (1994).
727 72 D. Hobbs, G. Kresse, and J. Hafner, *Phys. Rev. B* **62**,
728 11556 (2000).
729 73 H. J. Monkhorst and J. D. Pack, *Phys. Rev. B* **13**, 5188
730 (1976).
731 74 M. Gajdoš, K. Hummer, G. Kresse, J. Furthmüller, and
732 F. Bechstedt, *Phys. Rev. B* **73**, 045112 (2006).
733 75 J. Buckeridge, A. M. Teweldeberhan, and S. Fahy, *Phys.*
734 *Rev. B* **79**, 153201 (2009).
735 76 J. Buckeridge and S. Fahy, *Phys. Rev. B* **84**, 144120
736 (2011).
737 77 J. Buckeridge, S. O'Halloran, and S. Fahy, *Solid State*
738 *Commun.* **150**, 1967 (2010).
739 78 S. B. Zhang and J. E. Northrup, *Phys. Rev. Lett.* **67**,
740 2339 (1991).
741 79 C. Freysoldt, B. Grabowski, T. Hickel, J. Neugebauer,
742 G. Kresse, A. Janotti, and C. G. Van de Walle, *Rev.*
743 *Mod. Phys.* **86**, 253 (2014).
744 80 S. Lany and A. Zunger, *Phys. Rev. B* **78**, 235104 (2008).
745 81 T. R. Durrant, S. T. Murphy, M. B. Watkins, and A. L.
746 Shluger, *J. Chem. Phys.* **149**, 024103 (2018).
747 82 J. Buckeridge, D. O. Scanlon, A. Walsh, and C. R. A.
748 Catlow, *Comput. Phys. Commun.* **185**, 330 (2014).
749 83 D. R. Lide, editor, *CRC handbook of Chemistry and*
750 *Physics*, CRC Press, Boca Raton, FL, 89th edition, 2008.
751 84 If we were to use the experimental heats of formation,
752 there would be no significant difference in our conclusions.
753 85 J. Buckeridge, <https://github.com/projects/sc-fermi.git>,
754 2016.
755 86 F. H. Taylor, J. Buckeridge, and C. R. A. Catlow, *Chem.*
756 *Mater.* **28**, 8210 (2016).
757 87 J. Buckeridge, D. Jevdokimovs, C. R. A. Catlow, and
758 A. A. Sokol, *Phys. Rev. B* **94**, 180101(R) (2016).
759 88 J. Buckeridge, *Comput. Phys. Commun.* (In press) (2019).
760 89 N. N. Sirota and F. M. Gololobov, *Dokl. Akad. Nauk*
761 *SSSR* **144**, 398 (1962).
762 90 H. J. McSkimin, A. Jayaraman, J. P. Andreatch, and
763 T. B. Bateman, *J. Appl. Phys.* **39**, 4127 (1968).
764 91 W. F. Boyle and R. J. Sladek, *Phys. Rev. B* **11**, 2933
765 (1975).
766 92 M. Wu and C. Chen, *J. Appl. Phys.* **72**, 4275 (1992).
767 93 T. C. Chiang and D. E. Eastman, *Phys. Rev. B* **22**, 2940
768 (1980).
769 94 D. Hill and C. Schwerdtfeger, *J. Phys. Chem. Solids* **35**,
770 1533 (1974).
771 95 M. W. Heller and R. G. Hamerly, *J. Appl. Phys.* **57**, 4626
772 (1985).
773 96 K. Aoki, E. Anastassakis, and M. Cardona, *Phys. Rev. B*
774 **30**, 681 (1984).
775 97 I. Vurgaftman, J. R. Meyer, and L. R. Ram-Mohan, *J.*
776 *Appl. Phys.* **89**, 5815 (2001).
777 98 L. J. Slutsky and C. W. Garland, *Phys. Rev.* **113**, 167
778 (1959).
779 99 C. L. Littler and D. G. Seiler, *Appl. Phys. Lett.* **46**, 986
780 (1985).
781 100 W. Zawadzki, *Advances in Phys.* **23**, 435 (1974).
782 101 D. L. Price, J. M. Rowe, and R. M. Nicklow, *Phys. Rev.*
783 *B* **3**, 1268 (1971).
784 102 G. P. Williams, F. Cerrina, G. J. Lapeyre, J. R. Anderson,
785 R. J. Smith, and J. Hermanson, *Phys. Rev. B* **34**, 5548

- (1986).
- ⁷⁸⁶ ¹⁰³ H. U. Middelmann, L. Sorba, V. Hinkel, and K. Horn,
⁷⁸⁷ Phys. Rev. B **34**, 957 (1986).
⁷⁸⁸
- ⁷⁸⁹ ¹⁰⁴ J. W. Kim, S. Kim, J. M. Seo, S. Tanaka, and M. Kamada,
⁷⁹⁰ J. Phys: Condens. Matter **8**, 4189 (1996).
⁷⁹¹ ¹⁰⁵ M. Shishkin and G. Kresse, Phys. Rev. B **74**, 035101
⁷⁹² (2006).
⁷⁹³ ¹⁰⁶ M. Shishkin and G. Kresse, Phys. Rev. B **75**, 235102
⁷⁹⁴ (2007).
⁷⁹⁵ ¹⁰⁷ M. Shishkin, M. Marsman, and G. Kresse, Phys. Rev.
⁷⁹⁶ Lett. **99**, 246403 (2007).
- ⁷⁹⁷ ¹⁰⁸ P. Y. Yu and M. Cardona, *Fundamentals of Semiconduc-*
⁷⁹⁸ *tors*, chapter 2, Springer, third edition, 2005.
⁷⁹⁹ ¹⁰⁹ N. Segercrantz, J. Slotte, F. Tuomisto, K. Mizohata, and
⁸⁰⁰ J. Räsänen, Phys. Rev. B **95**, 184103 (2017).
⁸⁰¹ ¹¹⁰ D. L. Kendall and R. A. Huggins, J. Appl. Phys. **40**, 2750
⁸⁰² (1969).
⁸⁰³ ¹¹¹ A. N. Morozov, T. V. Abaeva, and V. T. Bublik, Cryst.
⁸⁰⁴ Res. Technol. **21**, 613 (1986).
⁸⁰⁵ ¹¹² J. Xin, Q. Jiang, Y. Wen, S. Li, J. Zhang, A. Basit, L. Shu,
⁸⁰⁶ X. Li, and J. Yang, J. Mater. Chem. A **6**, 17049 (2018).
⁸⁰⁷ ¹¹³ R. Magri and A. Zunger, Phys. Rev. B **65**, 165302 (2002).